INDEX COPERNICUS INTERNATIONAL

Bio-Algorithms and Med-Systems

WWW.BAMSJOURNAL.COM ISSN: 1896-530X

ORIGINAL ARTICLE

Received: 26.11.2023
Accepted: 20.12.2023
Published: 31.12.2023

CITE THIS ARTICLE AS:
Parzych S, "Optimization of positronium imaging performance of a simulated modular J-PET scanner using GATE software," Bio-Algorithms and Med-Systems vol. 19, no. 1, pp. 80-86, 2023, DOI: 10.5604/01.3001.0054.1937

AUTHORS' CONTRIBUTION:
A – Study Design
B – Data Collection
C – Statistical Analysis
D – Data Interpretation
E – Manuscript Preparation
F – Literature Search
G – Funds Collection

CORRESPONDING AUTHOR:
Szymon Parzych; M. Smoluchowski Institute of Physics, Faculty of Physics, Astronomy and Applied Computer Science, Jagiellonian University, Krakow, Poland; Łojasiewicza street 11, 30-348 Krakow, Poland; E-mail: szymon.parzych@doctoral.uj.edu.pl

Optimization of positronium imaging performance of a simulated modular J-PET scanner using GATE software

Szymon Parzych[1,2,3ABCDEFG]

[1]M. Smoluchowski Institute of Physics, Faculty of Physics, Astronomy and Applied Computer Science, Jagiellonian University, Krakow, Poland
[2]Total-Body Jagiellonian-PET Laboratory, Jagiellonian University, Krakow, Poland
[3]Centre for Theranostics, Jagiellonian University, Krakow, Poland

ABSTRACT

Recently, a novel PET imaging method – positronium imaging – has been proposed to take advantage of previously unused information about the positronium states. The first *ex-vivo* and *in-vivo* images of positronium characteristics were acquired with the J-PET tomograph. Complementary to the standard annihilation photon's detection, positronium imaging also requires the registration of the prompt photon, which follows β+ decay. To that end, the introduction of an additional energy threshold for prompt γ registration and optimization of the energy window for annihilation γ are required. This simulation-based work undertook the mentioned task in the case of the modular J-PET scanner. Based on the ^{44}Sc radioisotope, the energy window for annihilation photons was established to 0.2 MeV – 0.37 MeV, while the threshold for prompt gamma was fixed at 0.37 MeV, closely following the end of the energy window for annihilation photons.

KEYWORDS

positronium imaging, multiphoton PET imaging, J-PET, simulation, GATE, energy window, ^{44}Sc

INTRODUCTION

Positronium imaging [1] is gaining interest as a novel PET imaging method that may enhance standard metabolic PET tomography by providing complementary information about the imaging tissue [2, 3]. It takes advantage of previously unused information about the metastable states of positronium, e.g. mean lifetime or formation probability, which can be utilized as biomarkers and is qualitatively different from the traditional standardized uptake value (SUV) [1, 2, 4, 5]. Recently, the first 3γ ortho-positronium images [6] and both *ex-vivo* [7] and *in-vivo* [8] positronium life-time images were demonstrated with the Jagiellonian-PET (J-PET) tomograph, which

present an unconventional approach and design to PET scanner's construction by means of organic scintillators [9, 10]. Simultaneously, novel techniques for analysis of positronium lifetime spectra and positronium imaging reconstruction algorithms are emerging [11–15], indicating worldwide interest in this imaging method. Moreover, the apparent issue of low sensitivity to such imaging due to requirement of three photons coincidence, which causes degradation in the probability of event detection, can be addressed by the utilization of high-sensitivity PET scanners, namely the total-body PET tomographs [16–18]. The registration of triple coincidence events is also gaining interest in view of double tracer imaging [19–27].

Traditional metabolic imaging focuses on registration of the back-to-back photons originating from the e^+e^- annihilation and of energy 0.511 MeV each. To that end, in J-PET systems an energy threshold is being used to, e.g. minimize the detection of photons' scatterings [28]. Due to the necessity of the additional registration of deexcitation (prompt) photons in positronium imaging, a second energy threshold has to be introduced. This second threshold is, however, associated with limiting the energy region for choosing annihilation photons and converting it into an energy window (described in detail in the Energy-window technique subsection of the Methods section).

In this simulation-based work, abovementioned energy thresholds (windows) will be examined to maximize the quality of the data taken with the modular J-PET tomograph and to set new guidelines for real-data analysis of positronium imaging. The ^{44}Sc radioisotope has been chosen for this consideration due to its feasibility for positronium imaging [29]. The simplified decay scheme of a ^{44}Sc scandium isotope with a focus on the positronium-oriented decay channel is presented in Fig. 1.

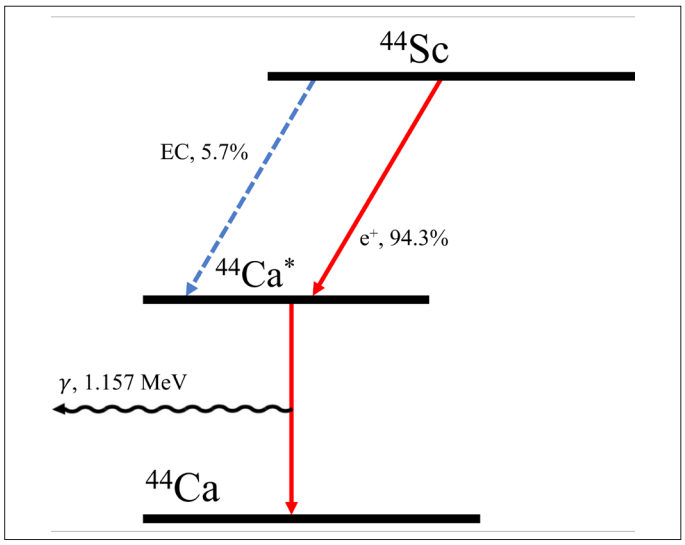

Fig. 1. The decay scheme for the ^{44}Sc radioisotope. The presented scheme focuses on the positronium-oriented decay channel (denoted by the e^+). Additionally, EC indicates the electron capture contribution.

METHODS

Simulation setup

This simulation-based study was performed by means of Geant4 Application for Tomographic Emission (GATE) software, version 9.0. This advanced, opensource software allows for generation of radioactive source decays and investigation of interactions of their products, together with simulation of the PET scanners and their responses [30, 31].

This research is dedicated to the modular J-PET scanner [10, 32]. Its simulation counterpart consists of 24 detection modules arranged into a 1-layer ring with a 74-cm inner diameter. Each module is formed from 13 axially arranged plastic scintillator strips with dimensions of 24 × 6 × 500 mm^3, read out on both ends by electronic systems [32, 33].

The investigation performed during this study concentrates on positronium imaging. Due to that, during simulation, a source which produces 2 annihilation photons and 1 deexcitation (prompt) photon had to be simulated. In its new version, a recent update to GATE software [30, 31] introduced models of generation of such radioactive sources: para-positronium (p-Ps), ortho-positronium (o-Ps) and mixed positronium (Ps). The most useful for diagnostic purposes is ortho-positronium [2, 3, 34, 35], which decays into three photons in a vacuum. However, in the tissue, due to the o-Ps-p-Ps conversion or pickoff processes, the annihilation leads to the emission of two photons instead of three. Since GATE is not simulating such processes, the p-Ps source, which leads to a two-photon emission, was chosen. Nevertheless, it is possible to exchange its built-in mean lifetime value – 125 ps (mean lifetime in the vacuum [36]) – to more closely reflect the o-Ps state. Further, a prompt gamma emission of chosen energy (1.157 MeV) was added. By default, emission of all photons is isotropic and was left as such. After generation, each gamma was tracked, and while encountering any material (phantom, crystals, etc.) the GATE software simulates the possible interactions (e.g. photo-effect, Compton scattering). Cross-sections for each are already preprogrammed in GATE.

Energy window technique

During metabolic imaging in plastic-based PET scanners, the registration of the e^+e^- annihilation, back-to-back photons within the scintillators occurs via the Compton effect. Due to lack of the 0.511 MeV photopeak, a standard energy window which allows rejection of part of the photons which already underwent any scattering (e.g. in the patient's body), and registration of which degrades the quality of the imaging, is limited to an energy threshold (see Fig. 2., left). The value of that threshold was previously studied and estimated to 0.2 MeV [28, 33].

In case of the detection of prompt photons in positronium imaging, whose energies are higher than 0.511 MeV and their Compton edge

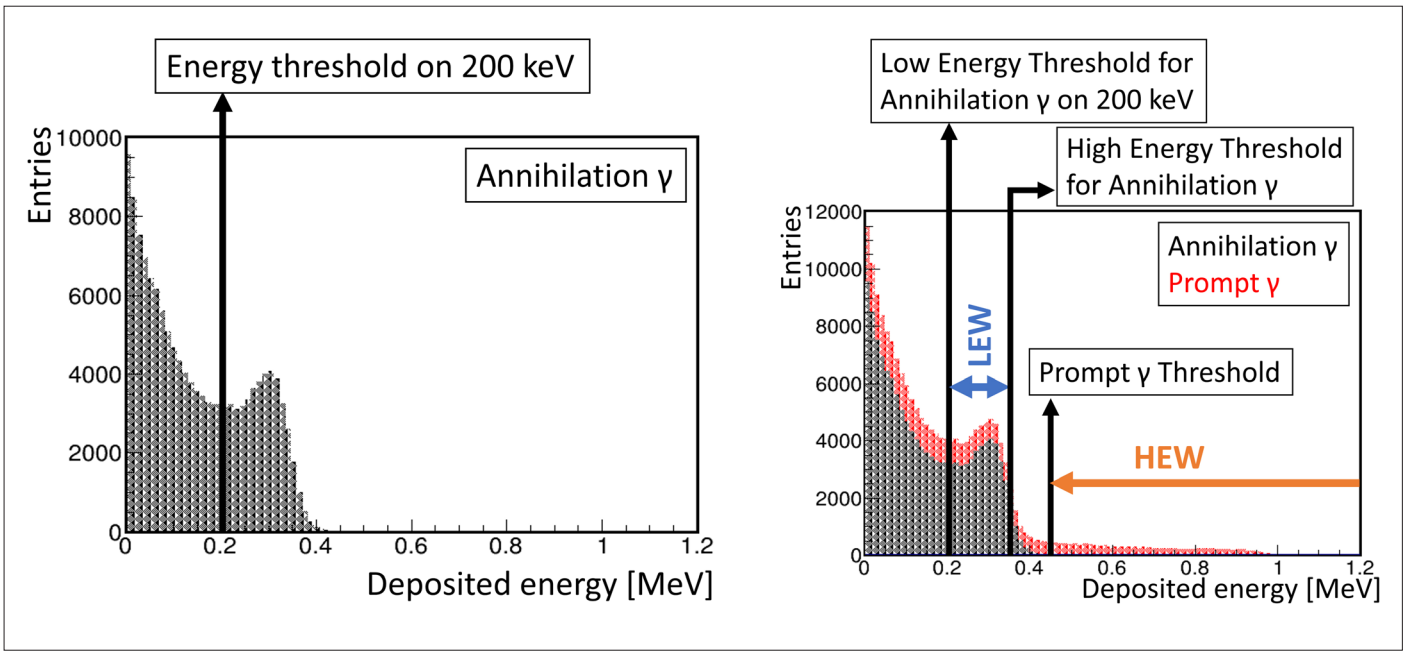

Fig. 2. Left, spectrum of the energy deposition of 0.511 MeV photons originating from positronium annihilation inside the plastic scintillator, obtained with the simulated modular J-PET setup. The vertical arrow marks the previously established 0.2 MeV threshold [28, 33]. Right, the energy deposition spectrum of annihilation photons (black) and prompt photons (red) is simulated from the ^{44}Sc decays. Vertical arrows mark all three energy limits, denoted by their introduced names. Moreover, ranges of the Lower Energy Window (blue) and Higher Energy Window (orange) are indicated with horizontal arrows. During the simulation all deposited energies were smeared according to Gaussian distribution, where its full width at half maximum (represented by resolution) was calculated following the inverse square law. For the investigated system a resolution of 23% was set at energy equal to 0.2 MeV [33].

is further on the energy spectrum (see Fig. 2., right), a new energy threshold has to be specifically applied for them. However, introduction of the second threshold puts constraint on the energy region for annihilation photon candidates, involuntarily transforming the first energy threshold into an energy window. Moreover, assuming a high enough second energy threshold so that none of the annihilation photons can exceed it, the upper limit of the energy window may have to be lower. This hypothesis introduces in total 2 new energy limits, the estimation of which is undertaken in this work. Henceforth, a new naming system will be introduced (see Fig. 2., right):

- The previous energy threshold on 0.2 MeV will be denoted as the Low Energy Threshold for Annihilation γ (stable during whole research);
- The newly created energy window for annihilation photon candidates will be called the Lower Energy Window (LEW);
- The upper limit of the LEW is denoted as the High Energy Threshold for Annihilation γ;
- The second energy threshold for prompt photon candidates is named the Prompt γ Threshold;
- The resulting infinite energy window, starting from the Prompt γ Threshold, is called the Higher Energy Window (HEW). The HEW from its upper side can be left open since there are no other, even more energetic photons, being simulated.

In order to find the optimal High Energy Threshold for Annihilation γ and Prompt γ Threshold, two simulations were conducted under the condition involving the use and absence of a phantom.

1. A 183-cm linear source situated at the trans-axial centre and along the central axis of the tomograph with 1 MBq activity;
2. A water-filled cylinder of a radius equal to 10.6 cm and 168 cm in length (corresponding to BMI = 22.6 [37]) with uniformly distributed 1 MBq activity, situated centrally within the scanner.

Coincidence sorting has been performed assuming a time window of 3 ns. Moreover, each interaction falling into coincidence had to be registered with a different module of the modular J-PET system.

RESULTS

Gamma selection quality

Utilization of the energy window allows us to separate the gathered data into two subgroups: coming from the interaction of annihilation or prompt γ. Additionally, it preliminary rejects part of the possible scattered data. In the case of standard 2γ imaging with a β^+ emitter, the purity of such selection is undisturbed due to lack of deexcitation photons, while its efficiency is dictated only by the width of the energy window. However, if one introduces a radioisotope, which deexcites with the emission of an additional

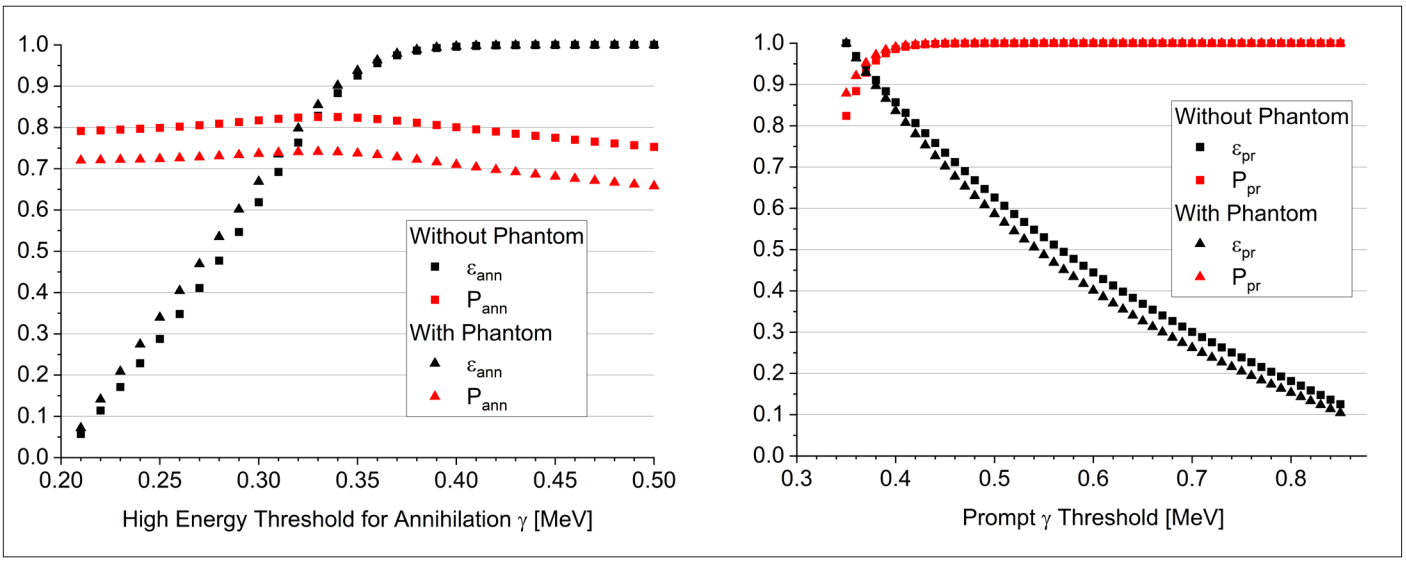

Fig. 3. Left, dependence of the efficiency ε_{ann} (black) and purity P_{ann} (red) of choosing annihilation γ in the LEW on the value of the High Energy Threshold for Annihilation γ. The efficiency has been defined as a number of annihilations γ in the LEW to all annihilations γ above 0.2 MeV, while purity is defined as the number of annihilations to all photons in the LEW. Right, the dependence of efficiency ε_{pr} (black) and purity P_{pr} (red) for choosing prompt γ from the HEW on the value of the Prompt γ Threshold. The efficiency has been defined as a number of prompts γ from the HEW to all prompts γ above 0.35 MeV; purity is analogous, as before. In both plots the results of the simulations with and without phantoms are marked as triangles and rectangles, respectively.

photon after β+ decay, the energy spectra of both types of gammas may overlap (see Fig. 2., right), deteriorating the selection's purity. By means of efficiency and purity, Fig. 3. shows the quality of energy window technique for both annihilations γ in the LEW (left) and prompt γ in the HEW (right) for given energy thresholds. The presented results for the High Energy Threshold for Annihilation γ show an almost linear increase in the efficiency of the annihilation gamma registration (ε_{ann}) up to ~0.35 MeV, where the trend slows to soon reach maximum. At the same time, purity remains approximately stable, with a slight peak in the 0.30–0.38 MeV region. These outcomes suggest possible region of interest for the High Energy Threshold for Annihilation γ selection. In the case of the Prompt γ Threshold, the purity is saturated quickly; however, the efficiency of prompt registration (ε_{pr}) is rapidly falling.

Double coincidences

The base for both metabolic and positronium imaging is the registration of two annihilation photons in coincidence in the LEW to create a candidate pair for further studies. Unfortunately, the utilization of $\beta^+ + \gamma$ radioisotopes introduces the possibility of detecting wrong candidate pairs, e.g. 'annihilation γ + prompt γ' or 'prompt γ + prompt γ'. These false candidates greatly impact the quality of the final image due to their misleading information about the e^+e^- annihilation position. Fig. 4. (left) shows the probability (purity) of selecting the true candidate pairs (P_{pair}), and an additional figure of merit ($FoM_{pair,\varepsilon}$) depicting the influence of the statistics on the former by the means of taking into account the ε_{ann}. The $FoM_{pair,\varepsilon}$ is defined as:

$$FoM_{pair,\varepsilon} = P_{pair} \times \varepsilon_{ann} .$$

Due to the multiplication of parameters in the ranges of ⟨0, 1⟩, the resulting figure of merit can also take values in the ⟨0, 1⟩ region, where higher value corresponds to better signal. The obtained graphs indicate the best performance of the LEW, with its upper limit at 0.37 MeV.

Subsequently to choosing true candidate pairs, they are further divided into standard types of coincidences, namely: true, phantom scattered, detector scattered and accidental (random) coincidences. The latter represents a pair of annihilation photons originating from different annihilation events. Both scattered coincidences denote the situation in which prior to registration the annihilation gamma underwent other interactions within the phantom (body) or the scintillators themselves. The manipulation of the width of the LEW impacts the probability of registration of different types of coincidences: true (P_t), phantom scattered (P_{ps}), detector scattered (P_{ds}) and accidental (P_r). However, for the sake of final image quality, the ratios between degradable and true coincidences are essential. Therefore, the following ratios have been investigated and shown in Fig. 5.

$$R_{ds} = \frac{P_{ds}}{P_t} ,$$

$$R_{ps} = \frac{P_{ps}}{P_t} .$$

The influence on random coincidences was neglected due to their uniform distribution. The resulting plots point out that above 0.33 MeV there is no significant difference in between the difference in ratio of gathered scattered to true coincidences.

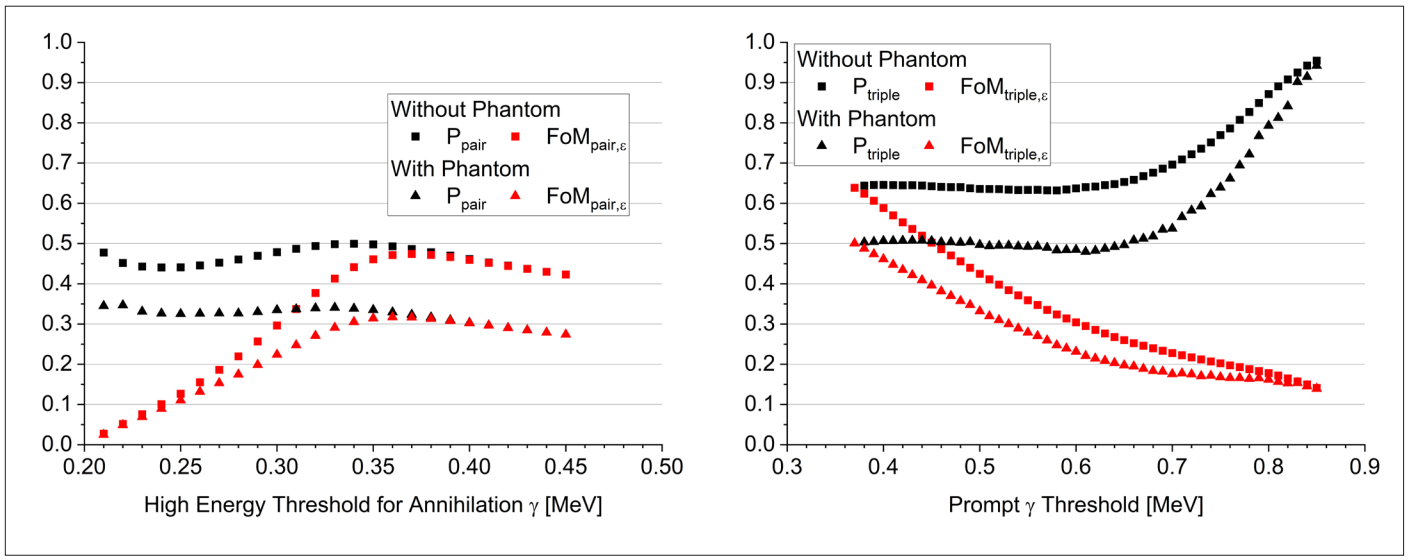

Fig. 4. Left, dependence of probability of detecting the true candidate pairs P_{pair} (black) and figure of merit $FoM_{pair,\varepsilon}$ (red) on the value of the High Energy Threshold for Annihilation γ. Right, the dependence of probability of detecting the true candidate triples P_{triple} (black) and figure of merit $FoM_{triple,\varepsilon}$ (red) on the value of the Prompt γ Threshold. In both plots the result of simulations with and without a phantom are marked as triangles and rectangles, respectively.

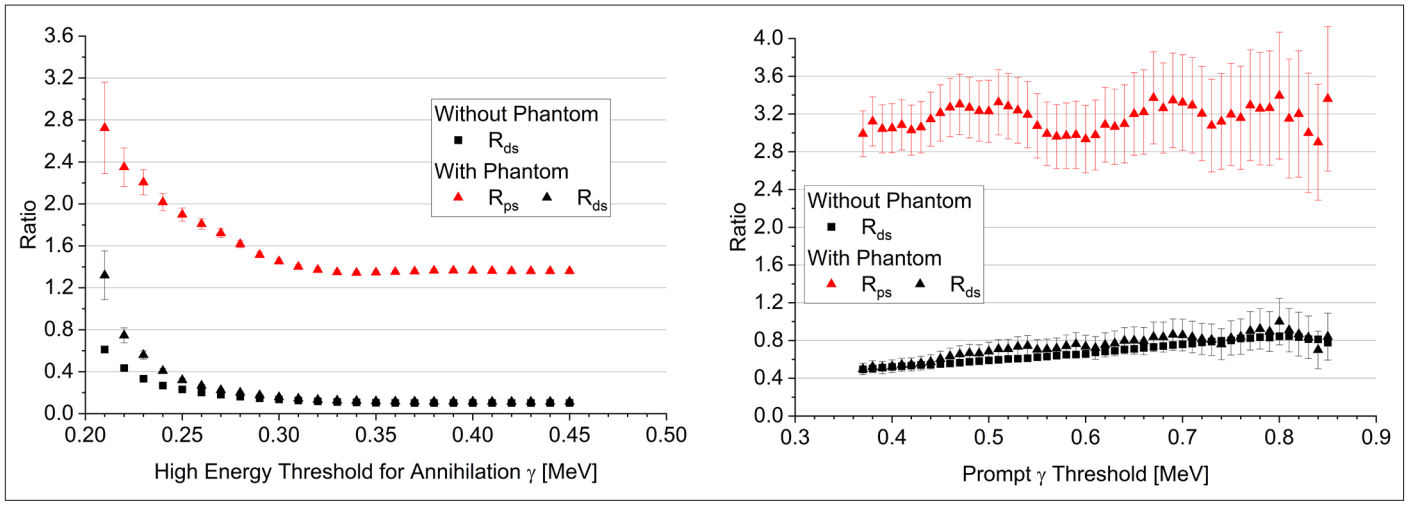

Fig. 5. Plots portray ratios between detector scattered and true coincidences (R_{ds}, black), and phantoms scattered and true coincidences (R_{ps}, red) for double coincidences in the LEW (left) and triple coincidences assuming different HEWs (right). In both plots the result of simulations with and without phantoms are marked as triangles and rectangles, respectively.

The definitive optimization of the High Energy Threshold for Annihilation γ positioning was done by introducing the next two figures of merit, which take into account the probability (purity) of choosing true candidate pairs (P_{pair}), true coincidences (P_t) and statistics (ε_{ann}). Their definitions are as follows:

$$FoM_{pair,type} = P_{pair} \times P_t \,,$$

$$FoM_{pair,type,\varepsilon} = P_{pair} \times P_t \times \varepsilon_{ann} \,.$$

Similarly, as previously, the resulting figures of merit can take values in the ⟨0, 1⟩ region, where the higher value corresponds to a better signal. The obtained dependencies are shown in Fig. 6. (left), clearly indicating the best performance at the 0.37 MeV threshold, which also falls into the plateau region of R_{ds} and R_{ps}. The 0.37 MeV High Energy Threshold for Annihilation γ will be used in further studies.

Triple coincidences

Positronium imaging requires the registration of additional, more energetic prompt photons, which falls into the Higher Energy Window. A candidate pair from the LEW and another candidate from the HEW create a candidate triple. Similarly, as before, due to overlapping energy spectra of annihilation and prompt photon, there is a possibility of detection of improper candidate triples: '2×annihilation γ + prompt γ', '2×annihilation γ + annihilation γ', 'annihilation γ + prompt γ + prompt γ', etc. Fig. 4. (right) shows

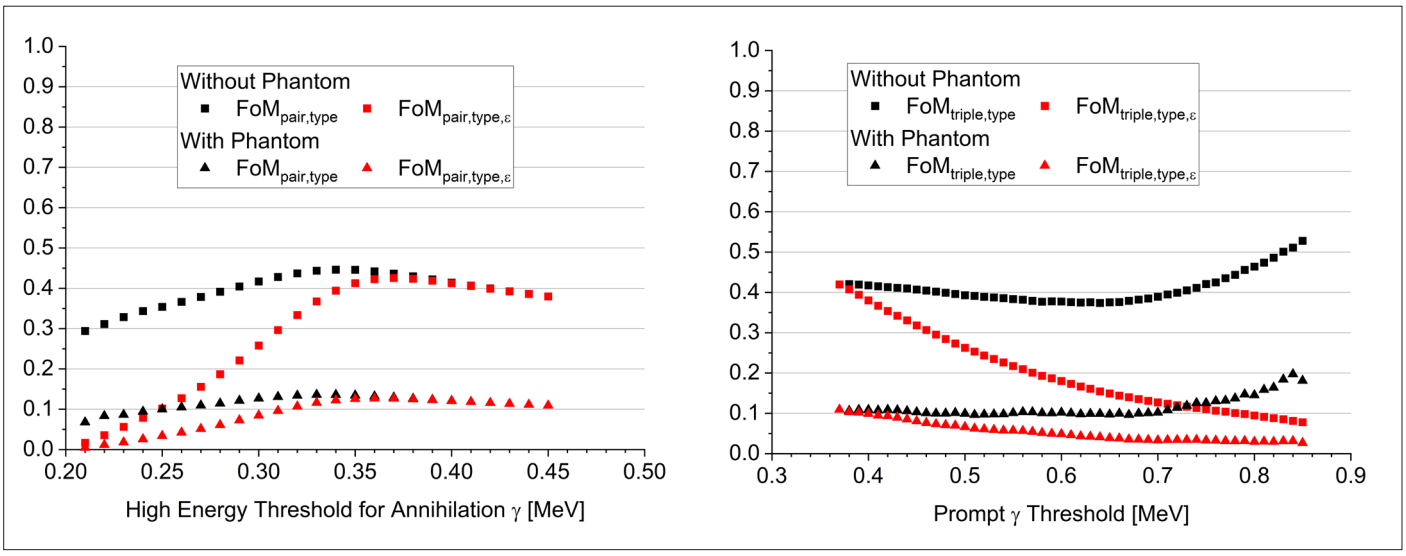

Fig. 6. Left, the dependence of figures of merit $FoM_{pair,type}$ (black) and $FoM_{pair,type,\varepsilon}$ (red), which take into account the probability of choosing true candidate pairs P_{pair}, true coincidences P_t and statistics ε_{ann}, on the value of the High Energy Threshold for Annihilation γ. Right, the dependence of figures of merit $FoM_{triple,type}$ (black) and $FoM_{triple,type,\varepsilon}$ (red), which take into account the probability of choosing true candidate triples P_{triple}, true coincidences P_t and statistics ε_{pr}, on the value of the Prompt γ Threshold. In both plots the results of simulations with and without phantoms are marked as triangles and rectangles, respectively.

the probability (purity) of selecting the true candidate triples (P_{triple}) and corresponding figure of merit ($FoM_{triple,\varepsilon}$), defined as:

$$FoM_{triple,\varepsilon} = P_{triple} \times \varepsilon_{pr} \ .$$

The obtained plot shows a clear downward trend in $FoM_{triple,\varepsilon}$, which suggests best performance at the lowest possible Prompt γ Threshold.

Furthermore, each candidate triple can be divided into aforementioned types of coincidences. Fig. 5. (right) presents ratios between false and true coincidences demonstrating a slight growing trend, hinting towards a worse yield for a higher threshold. Ultimately, final figures of merit are introduced as follows:

$$FoM_{triple,type} = P_{triple} \times P_t \ ,$$

$$FoM_{triple,type,\varepsilon} = P_{triple} \times P_t \times \varepsilon_{pr} \ ,$$

depicting the joint probability (purity) of choosing true candidate triples and true coincidences, and also taking into account the statistics of qualifying prompt photons. The obtained results are shown in Fig. 6. (right), once more pointing to the best performance with a Prompt γ Threshold equal to the High Energy Threshold for Annihilation γ – 0.37 MeV.

CONCLUSIONS

The presented study discussed the importance of the utilization of adequate energy windows for the registration of annihilation and deexcitation photons in positronium imaging. This simulation-based investigation has been performed for the modular J-PET tomograph from the J-PET collaboration.

The examination consisted of optimizing the upper limit of the energy window for annihilation γ detection, as well as the energy threshold for selecting prompt γ. Demonstrated analysis and results suggest that the most optimal configuration of the abovementioned thresholds is identical for both and equal to 0.37 MeV. Although the analysed step in thresholds was equal to 0.01 MeV, the possible deviation from the selected energy for the most optimal solution was not essential. Due to the fact that PET tomographs constructed with the J-PET technology work in the Time-over-Threshold (TOT) system, the optimal value of the threshold found from the simulation has to be converted to the TOT [38]. Since such conversion is dictated by the energy–TOT calibration with its own uncertainty, the variation in the optimal energy can be neglected. Moreover, the obtained result is in close agreement with the previously studied energy-based selection of ^{44}Sc products for sparse multilayer J-PET geometry [39], which points to the generality of selected thresholds in all J-PET systems.

ACKNOWLEDGEMENTS

This work was supported by the Foundation for Polish Science through TEAM POIR 04.04.00-00-4204/17, and the National Science Centre, Poland (NCN) through grant nos. 2021/42/A/ST2/00423 and 2021/43/B/ST2/02150, and the SciMat and qLife Priority Research Area budget under the program Excellence Initiative – Research University, at Jagiellonian University.

REFERENCES

1. Moskal P. Positronium imaging. In: 2019 IEEE Nuclear Science Symposium and Medical Imaging Conference (NSS/MIC). Manchester, UK: IEEE Xplore; 2020.
2. Moskal P, Jasińska B, Stępień EŁ, Bass SD. Positronium in medicine and biology. Nat Rev Phys 2019;1:527-9.
3. Bass SD, Mariazzi S, Moskal P, Stępień E. Colloquium: Positronium physics and biomedical applications. Rev Mod Phys 2023;95:021002.
4. Moskal P, Kisielewska D, Curceanu C, Czerwiński E, Dulski K, Gajos A, et al. Feasibility study of the positronium imaging with the J-PET tomograph. Phys Med Biol 2019;64:055017.
5. Moskal P, Kisielewska D, Y Shopa R, Bura Z, Chhokar J, Curceanu C, et al. Performance assessment of the 2γ positronium imaging with the total-body PET scanners. EJNMMI Phys 2020;7:1-16.
6. Moskal P, Gajos A, Mohammed M, Chhokar J, Chug N, Curceanu C, et al. Testing CPT symmetry in ortho-positronium decays with positronium annihilation tomography. Nat Commun 2021;12:5658.
7. Moskal P, Dulski K, Chug N, Curceanu C, Czerwiński E, Dadgar M, et al. Positronium imaging with the novel multiphoton PET scanner. Sci Adv 2021;7:eabh4394.
8. Moskal P. The first in-vivo positronium imaging of the human brain. In: 2022 IEEE Nuclear Science Symposium and Medical Imaging Conference (NSS/MIC). Milano, Italy; 2022.
9. Niedźwiecki S, Białas P, Curceanu C, Czerwiński E, Dulski K, Gajos A, et al. J-PET: A New Technology for the Whole-body PET Imaging. Acta Phys Pol B 2017;48:1567-76.
10. Moskal P, Kowalski P, Shopa RY, Raczyński L, Baran J, Chug N, et al. Simulating NEMA characteristics of the modular total-body J-PET scanner – an economic total-body PET from plastic scintillators. Phys Med Biol 2021;66:175015.
11. Dulski K. PALS Avalanche – A New PAL Spectra Analysis Software. Acta Phys Pol A 2020;137:167.
12. Shibuya K, Saito H, Tashima H, Yamaya T. Using inverse Laplace transform in positronium lifetime imaging. Phys Med Biol 2022;67:025009.
13. Qi J, Huang B. Positronium Lifetime Image Reconstruction for TOF PET. IEEE Trans. Med. Imaging 2022;41:2848.
14. Zhu Z, Kao C-M, Huang H-H. A statistical reconstruction algorithm for positronium lifetime imaging using time-of-flight positron emission tomography. 2022; arXiv:2206.06463v3.
15. Shopa R, Dulski K. Multi-photon time-of-flight MLEM application for the positronium imaging in J-PET. Bio-Algorithms and Med-Systems 2022;18:135-43.
16. Badawi RD, Shi H, Hu P, Chen S, Xu T, Price PM, et al. First Human Imaging Studies with the EXPLORER Total-Body PET Scanner. J Nucl Med. 2019;60:299-303.
17. Karp JS, Viswanath V, Geagan MJ, Muehllehner G, Pantel AR, Parma MJ, et al. PennPET Explorer: Design and Preliminary Performance of a Whole-Body Imager. J Nucl Med. 2020;61:136-43.
18. Prenosil GA, Sari H, Fürstner M, Afshar-Oromieh A, Shi K, Rominger A, et al. Performance Characteristics of the Biograph Vision Quadra PET/CT System with a Long Axial Field of View Using the NEMA NU 2-2018 Standard. J Nucl Med. 2022;63:476-84.
19. Pratt EC, Lopez-Montes A, Volpe A, Crowley MJ, Carter LM, Mittal V, et al. Simultaneous quantitative imaging of two PET radiotracers via the detection of positron–electron annihilation and prompt gamma emissions. Nat Biomed Eng. 2023;7(8):1028-39.
20. Fukuchi T, Shigeta M, Haba H, Mori D, Yokokita T, Komori Y, et al. Image reconstruction method for dual-isotope positron emission tomography. Journal of Instrum. 2021;16(01):P01035.
21. Shimazoe K, Uenomachi M. Multi-molecule imaging and inter-molecular imaging in nuclear medicine. Bio-Algorithms and Med-Systems 2022;18(1):127-34.
22. Uenomachi M, Shimazoe K, Takahashi H. A double photon coincidence detection method for medical gamma-ray imaging. Bio-Algorithms and Med-Systems 2022;18(1):120-6.
23. Sitarz M, Cussonneau JP, Matulewicz T, Haddad F. Radionuclide candidates for β+ + γ coincidence PET: an overview. Appl Radiat Isot. 2020;155:108898.
24. Matulewicz T. Radioactive nuclei for β+ +γ PET and theranostics: selected candidates. Bio-Algorithms and Med-Systems 2021;17(4):235-9. https://doi.org/10.1515/bams-2021-0142.
25. Grignon C. Nuclear medical imaging using β+γ coincidences from 44Sc radio-nuclide with liquid xenon as detection medium. Nucl Instr and Meth A 2007;571:142-5.
26. Thirolf PG, Lang C, Parodi K. Perspectives for Highly-Sensitive PET--Based Medical Imaging Using β+γ Coincidences. Acta Phys Polon A 2015;127:1441-44.
27. Lang C, Habs D, Parodi K, Thirolf PG. Sub-millimeter nuclear medical imaging with high sensitivity in positron emission tomography using β+γ coincidences. Journal of Instrum. 2014;9:P01008.
28. Kowalski P, Wiślicki W, Raczyński L, Alfs D, Bednarski T, Białas P, et al. Scatter Fraction of the J-PET Tomography Scanner. Acta Phys Polon B 2016;47:549.
29. Moskal P, Stępień E. Prospects and clinical perspectives of total body PET imaging using plastic scintillators. Pet Clin 2020;15:439-52.
30. Sarrut D, Bała M, Bardiès M, Bert J, Chauvin M, Chatzipapas K, et al. Advanced Monte Carlo simulations of emission tomography imaging systems with GATE. Phys Med Biol 2021;66:10TR03.
31. Sarrut D, Sarrut D, Arbor N, Baudier T, Borys D, Etxebeste A, Fuchs H, et al. The OpenGATE ecosystem for Monte Carlo simulation in medical physics. Phys Med Biol 2022;67:184001.
32. Coussat A, Krzemień W, Baran J, Parzych S. Development of the Normalization Method for the Jagiellonian PET Scanner. Acta Phys Pol A 2022;142:414.
33. Moskal P, Niedźwiecki S, Bednarski T, Czerwiński E, Kapłon Ł, Kubicz E, et al. Test of a single module of the J-PET scanner based on plastic scintillators. Nucl Instr and Meth A 2014;764:317-21.
34. Moskal P, Kubicz E, Grudzień G, Czerwiński E, Dulski K, Leszczyński B, et al. Developing a Novel Positronium Biomarker for Cardiac Myxoma Imaging. EJNMMI Phys 2023;10:22.
35. Jasińska B, Zgardzińska B, Chołubek G, Gorgol M, Wiktor K, Wysogld K, et al. Human tissues investigation using PALS technique. Acta Phys Pol B. 2017;48:1737-47.
36. Bass S D. QED and Fundamental Symmetries in Positronium Decays. Acta Phys Polon B 2019;50:1319.
37. Ghabrial A, Franklin DR, Zaidi H. A Monte Carlo simulation study of scatter fraction and the impact of patient BMI on scatter in long axial field--of-view PET scanners. Z Med Phys. 2021;31:305-15.
38. Sharma S, Chhokar J, Curceanu C, Czerwinski E, Dadgar M, Dulski K, et al. Estimating relationship between the time over threshold and energy loss by photons in plastic scintillators used in the J-PET scanner. EJNMMI Phys 2020;7:39.
39. Masełek R, Krzemień W, Klimaszewski K, Raczyński L, Kowalski P, Shopa R, Wiślicki W, et al. Towards 2+1 photon tomography: Energy-based selection of two 511 keV photons and a prompt photon with the J-PET scanner. 2018;arXiv:1803.00996.